Inorg. Chem. **2005**, *44*, 8156–8166

Oxidizing Intermediates from the Sterically Hindered Iron Salen Complexes Related to the Oxygen Activation by Nonheme Iron Enzymes

Takuya Kurahashi,[†] Yoshio Kobayashi,[‡] Shigenori Nagatomo,[†] Takehiko Tosha,[†] Teizo Kitagawa,[†] and Hiroshi Fujii*,[†]

Institute for Molecular Science & Okazaki Institute for Integrative Bioscience, National Institutes of Natural Sciences, Myodaiji, Okazaki, Aichi 444-8787, Japan, and The Institute of Physical and Chemical Research (RIKEN), Hirosawa, Wako, Saitama 351-0198, Japan

Received August 12, 2005

Oxidizing intermediates are generated from nonheme iron(III) complexes to investigate the electronic structure and the reactivity, in comparison with the oxoiron(IV) porphyrin π-cation radical (compound I) as a heme enzyme model. Sterically hindered iron salen complexes, bearing a fifth ligand Cl (**1**), OH_2 (**2**), OEt (**3**), and OH (**4**), are oxidized both electrochemically and chemically. Stepwise one-electron oxidation of **1** and **2** generates iron(III)–mono- and diphenoxyl radicals, as revealed by detailed spectroscopic investigations, including UV–vis, EPR, Mössbauer, resonance Raman, and ESIMS spectroscopies. In contrast to the oxoiron(IV) formation from the hydroxoiron(III) porphyrin upon one-electron oxidation, the hydroxo complex **4** does not generate oxoiron(IV) species. Reaction of **2** with *m*CPBA also results in the formation of the iron(III)–phenoxyl radical. One-electron oxidation of **3** leads to oxidative degradation of the fifth EtO ligand to liberate acetaldehyde even at 203 K. The iron(III)–phenoxyl radical shows high reactivity for alcoxide on iron(III) but exhibits virtually no reactivity for alcohols including even benzyl alcohol without a base to remove an alcohol proton. This study explains unique properties of mononuclear nonheme enzymes with Tyr residues and also the poor epoxidation activity of Fe salen compared to Mn and Cr salen compounds.

Introduction

A number of important oxidative transformations are carried out by iron enzymes utilizing dioxygen as an oxygen source.[1] A wide variety of coordination environments around the iron center in those enzymes generate distinct oxidizing intermediates, which are supposed to result in their intrinsic reactivities. The most important feature of oxidizing intermediates in determining reactivities is how oxidizing equivalents from dioxygen are distributed around an iron center. In the case of heme enzymes, for example, the electronic structure of the oxidizing intermediate is well documented to be the oxoiron(IV) porphyrin π-cation radical called compound I, with two oxidizing equivalents divided into the central iron and the surrounding porphyrin ligand.[2] On the other hand, the Fe_2O_2 diiron active site observed for the soluble diiron enzyme methane monooxygenase[3] retains two oxidizing equivalents divided on two iron centers, generating the $Fe^{IV}{}_2O_2$ diamond core.[4]

In contrast, mononuclear nonheme iron enzymes have long been a challenge on how oxidizing equivalents are held without an electron pool such as a porphyrin π-conjugation and a nearby iron atom. From this viewpoint, the iron-containing glycopeptide bleomycin has been extensively studied for a long time, and the only oxidizing intermediate detected to date is the $Fe^{III}-OOH$ form.[5] But recent works on the taurin:α-ketoglutarate-dependent dioxygenase (TauD), which has a mononuclear nonheme iron center facially coordinated by two histidines (His) and one asparaginic acid

* To whom correspondence should be addressed. E-mail: hiro@ims.ac.jp.
† National Institutes of Natural Sciences.
‡ RIKEN.

(1) See, for example: Lippard, S. J.; Berg, J. M. *Principles of Bioinorganic Chemistry*; University Science Books: New York, 1994.
(2) Sono, M.; Roach, M. P.; Coulter, E. D.; Dawson, J. H. *Chem. Rev.* **1996**, *96*, 2841−2887.
(3) Rosenzweig, A. C.; Frederick, C. A.; Lippard, S. J.; Nordlund, P. *Nature* **1993**, *366*, 537−543.
(4) (a) Lee, S.-K.; Nesheim, J. C.; Lipscomb, J. D. *J. Biol. Chem.* **1993**, *268*, 21569−21577. (b) Lee, S.-K.; Fox, B. G.; Froland, W. A.; Lipscomb, J. D.; Münck, E. *J. Am. Chem. Soc.* **1993**, *115*, 6450−6451. (c) Liu, K. E.; Valentine, A. M.; Wang, D.; Huynh, B. H.; Edmondson, D. E.; Salifoglou, A.; Lippard, S. J. *J. Am. Chem. Soc.* **1995**, *117*, 10174−10185. (d) Shu, L.; Nesheim, J. C.; Kauffmann, K.; Münck, E.; Lipscomb, J. D.; Que, L., Jr. *Science* **1997**, *275*, 515−518.

10.1021/ic051377e CCC: $30.25
Published on Web 10/01/2005

(Asp), provided compelling evidence for the oxoiron(IV) formation during oxygen activation.[6] In addition, several synthetic oxoiron(IV) species were successfully prepared from biomimetic nonheme model complexes,[7] which share a redox-innocent nitrogen coordination motif together with TauD. These epoch-making examples suggest that an nonheme oxoiron(IV) species could possibly be stabilized by the His coordination.

Another group of nonheme iron enzymes bear tyrosine (Tyr) residues, which also play an important role in catalysis in a more diverse manner due to a redox-noninnocent nature.[8] For example, in the case of the ribonucleotide reductase R2 protein,[9] the uncoordinated Tyr in close proximity to the diiron(III) core is converted to the tyrosyl radical upon dioxygen activation.[10] A coordinated Tyr residue is also found for mononuclear nonheme iron(III) enzymes such as protocatechuate 3,4-dioxygenase (3,4-PCD) bearing the His_2Tyr_2 coordination environment.[11] Strikingly different from most of the iron enzymes activating dioxygen on the iron center, 3,4-PCD is proposed to activate an iron-bound substrate for reaction with dioxygen.[12] A rather unique reaction sequence of 3,4-PCD is possibly induced by the electronic effect caused by the Tyr coordination to the iron(III) center.

Model studies concerning both coordinated and uncoordinated Tyr in nonheme iron enzymes have been quite limited so far.[13−15] To examine the Tyr coordination to the iron(III) center, Wieghardt et al. prepared a series of hexadentate iron complexes containing a 1,4,7-triazacyclononane backbone and three N-bound phenolate moieties.[14] Stepwise one-electron oxidation of their model complexes was reported to result in three successive ligand-centered, phenolate-to-phenoxyl radical conversions. Their phenoxyl radical complexes are excellent models, which are stable at room temperature. However, their model complexes do not necessarily reproduce the biological system in all aspects, because their model system does not have a vacant coordination site, which is critical for accommodation of a biologically important ligand such as H_2O and OH. Indeed, 3,4-PCD has a vacant coordination site, which is occupied with a solvent-derived water molecule.[11] The vacant coordination site on the iron(III) center would be of considerable importance for substrate-binding, considering the examples of the copper(II)−phenoxyl radical as a model for galactose oxidase (GO).[16] At present, reactivity of the iron(III)−phenoxyl radical intermediates is not clear.[14]

In this context, we constructed a biologically more relevant system based on a iron salen complex. A salen ligand well reproduces the coordination environment by two His and two Tyr. Most importantly, an iron salen complex has a vacant fifth coordination site. Following the strategy utilized in the heme enzyme model,[17] we introduced bulky mesityl groups to the salen framework to stabilize the monomeric iron center and successfully prepared a H_2O-coordinated iron salen complex, which not only duplicates the structural features around the iron(III) active site but also mimics the spectral characteristics of 3,4-PCD.[18] Herein, we carried out electrochemical and chemical oxidation of the iron salen complexes bearing Cl (**1**), OH_2 (**2**), OEt (**3**), and OH (**4**) as a fifth ligand (Figure 1). We also attempted *m*CPBA

(5) (a) Burger, R. M.; Kent, T. A.; Horwitz, S. B.; Münck, E.; Peisach, J. *J. Biol. Chem.* **1983**, *258*, 1559−1564. (b) Burger, R. M.; Blanchard, J. S.; Horwitz, S. B.; Peisach, J. *J. Biol. Chem.* **1985**, *260*, 15406−15409. (c) Sam, J. W.; Tang, X.-J.; Peisach, J. *J. Am. Chem. Soc.* **1994**, *116*, 5250−5256. (d) Absalon, M. J.; Wu, W.; Kozarich, J. W.; Stubbe, J. *Biochemistry* **1995**, *34*, 2076−2086. (e) Neese, F.; Zaleski, J. M.; Zaleski, K. L.; Solomon, E. I. *J. Am. Chem. Soc.* **2000**, *122*, 11703−11724.

(6) (a) Price, J. C.; Barr, E. W.; Tirupati, B.; Bollinger, J. M., Jr.; Krebs, C. *Biochemistry* **2003**, *42*, 7497−7508. (b) Proshlyakov, D. A.; Henshaw, T. F.; Monterosso, G. R.; Ryle, M. J.; Hausinger, R. P. *J. Am. Chem. Soc.* **2004**, *126*, 1022−1023. (c) Riggs-Gelasco, P. J.; Price, J. C.; Guyer, R. B.; Brehm, J. H.; Barr, E. W.; Bollinger, J. M., Jr.; Krebs, C. *J. Am. Chem. Soc.* **2004**, *126*, 8108−8109.

(7) (a) Grapperhaus, C. A.; Mienert, B.; Bill, E.; Weyhermüller, T.; Wieghardt, K. *Inorg. Chem.* **2000**, *39*, 5306−5317. (b) Rohde, J.-U.; In, J.-H.; Lim, M. H.; Brennessel, W. W.; Bukowski, M. R.; Stubna, A.; Münck, E.; Nam, W.; Que, L., Jr. *Science* **2003**, *299*, 1037−1039. (c) Lim, M. H.; Rohde, J.-U.; Stubna, A.; Bukowski, M. R.; Costas, M.; Ho, R. Y. N.; Münck, E.; Nam, W.; Que, L., Jr. *Proc. Natl. Acad. Sci. U.S.A.* **2003**, *100*, 3665−3670. (d) Balland, V.; Charlot, M.-F.; Banse, F.; Girerd, J.-J.; Mattioli, T. A.; Bill, E.; Bartoli, J.-F.; Battioni, P.; Mansuy, D. *Eur. J. Inorg. Chem.* **2004**, 301−308. (e) Kaizer, J.; Klinker, E. J.; Oh, N. Y.; Rohde, J.-U.; Song, W. J.; Stubna, A.; Kim, J.; Münck, E.; Nam, W.; Que, L., Jr. *J. Am. Chem. Soc.* **2004**, *126*, 472−473. (f) Decker, A.; Rohde, J.-U.; Que, L., Jr.; Solomon, E. I. *J. Am. Chem. Soc.* **2004**, *126*, 5378−5379. (g) Rohde, J.-U.; Torelli, S.; Shan, X.; Lim, M. H.; Klinker, E. J.; Kaizer, J.; Chen, K.; Nam, W.; Que, L., Jr. *J. Am. Chem. Soc.* **2004**, *126*, 16750−16761. (h) Ghosh, A.; Tiago de Oliveira, F. Yano, T.; Nishioka, T.; Beach, E. S.; Kinoshita, I.; Münck, E.; Ryabov, A. D.; Horwitz, C. P.; Collins T. J. *J. Am. Chem. Soc.* **2005**, *127*, 2505−2513. (g) Kim, S. O.; Sastri, C. V.; Seo, M. S.; Kim, J.; Nam, W. *J. Am. Chem. Soc.* **2005**, *127*, 4178−4179.

(8) Solomon, E. I.; Brunold, T. C.; Davis, M. I.; Kemsley, J. N.; Lee, S.-K.; Lehnert, N.; Neese, F.; Skulan, A. J.; Yang, Y.-S.; Zhou, J. *Chem. Rev.* **2000**, *100*, 235−349.

(9) Nordlund, P.; Sjöberg, B.-M.; Eklund, H. *Nature* **1990**, *345*, 593−598.

(10) Stubbe, J.; Donk, W. A. v. d. *Chem. Rev.* **1998**, *98*, 705−762.

(11) (a) Ohlendorf, D. H.; Lipscomb, J. D.; Weber, P. C. *Nature* **1988**, *336*, 403−405. (b) Ohlendorf, D. H.; Orville, A. M.; Lipscomb, J. D. *J. Mol. Biol.* **1994**, *244*, 586−608.

(12) Costas, M.; Mehn, M. P.; Jensen, M. P.; Que, L., Jr. *Chem. Rev.* **2004**, *104*, 939−986.

(13) Chaudhuri, P.; Wieghardt, K. *Prog. Inorg. Chem.* **2001**, *50*, 151−216.

(14) (a) Hockertz, J.; Steenken, S.; Wieghardt, K.; Hildebrandt, P. *J. Am. Chem. Soc.* **1993**, *115*, 11222−11230. (b) Adam, B.; Bill, E.; Bothe, E.; Goerdt, B.; Haselhorst, G.; Hildenbrand, K.; Sokolowski, A.; Steenken, S.; Weyhermüller, T.; Wieghardt, K. *Chem.*—Eur. *J.* **1997**, *3*, 308−319. (c) Snodin, M. D.; Ould-Moussa, L.; Wallmann, U.; Lecomte, S.; Bachler, V.; Bill, E.; Hummel, H.; Weyhermüller, T.; Hildebrandt, P.; Wieghardt, K. *Chem.*—Eur. *J.* **1999**, *5*, 2554−2565.

(15) (a) Goldberg, D. P.; Watton, S. P.; Masschelein, A.; Wimmer, L.; Lippard, S. J. *J. Am. Chem. Soc.* **1993**, *115*, 5346−5347. (b) Goldberg, D. P.; Koulougliotis, D.; Brudvig, G. W.; Lippard, S. J. *J. Am. Chem. Soc.* **1995**, *117*, 3134−3144.

(16) (a) Wang, Y.; Stack, T. D. P. *J. Am. Chem. Soc.* **1996**, *118*, 13097−13098. (b) Halfen, J. A.; Jazdzewski, B. A.; Mahapatra, S.; Berreau, L. M.; Wilkinson, E. C.; Que, L., Jr.; Tolman, W. B. *J. Am. Chem. Soc.* **1997**, *119*, 8217−8227. (c) Wang, Y.; DuBois, J. L.; Hedman, B.; Hodgson, K. O.; Stack, T. D. P. *Science* **1998**, *279*, 537−540. (d) Itoh, S.; Taki, M.; Takayama, S.; Nagatomo, S.; Kitagawa, T.; Sakurada, N.; Arakawa, R.; Fukuzumi, S. *Angew. Chem., Int. Ed.* **1999**, *38*, 2774−2776. (e) Chaudhuri, P.; Hess, M.; Müller, J.; Hildenbrand, K.; Bill, E.; Weyhermüller, T.; Wieghardt, K. *J. Am. Chem. Soc.* **1999**, *121*, 9599−9610. (f) Thomas, F.; Gellon, G.; Gautier-Luneau, I.; Saint-Aman, E.; Pierre, J.-L. *Angew. Chem., Int. Ed.* **2002**, *41*, 3047−3050.

(17) (a) Groves, J. T.; Haushalter, R. C.; Nakamura M.; Nemo, T. E.; Evans, B. J. *J. Am. Chem. Soc.* **1981**, *103*, 2884−2886. (b) Balch, A. L.; Latos-Grazynski, L.; Renner, M. W. *J. Am. Chem. Soc.* **1985**, *107*, 2983−2985. (c) Sugimoto, H.; Tung, H.-C.; Sawyer, D. T. *J. Am. Chem. Soc.* **1988**, *110*, 2465−2470. (d) Fujii, H. *J. Am. Chem. Soc.* **1993**, *115*, 4641−4648.

(18) Fujii, H.; Funahashi, Y. *Angew. Chem., Int. Ed.* **2002**, *41*, 3638−3641.

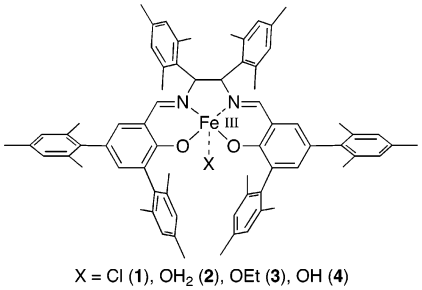

X = Cl (**1**), OH_2 (**2**), OEt (**3**), OH (**4**)

Figure 1. Series of iron salen complexes.

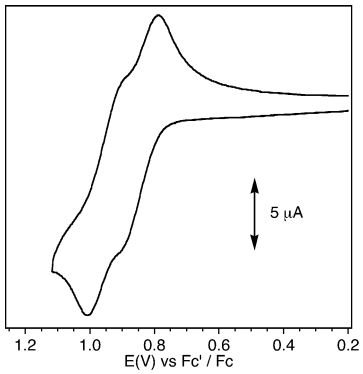

Figure 2. Cyclic voltammogram of **1** in CH_2Cl_2 at 233 K. Conditions: 1×10^{-3} M **1**; 0.10 M tetrabutylammonium perchlorate supporting electrolyte; a saturated calomel electrode as a reference electrode; a glassy carbon working electrode; a platinum-wire counter electrode; scan rate 50 mV s^{-1}. The potentials are referenced versus the ferrocenium/ferrocene (Fc′/Fc) couple.

oxidation of **2** to generate oxidizing intermediates, which is often utilized to generate high-valent metal−oxo species in porphyrin chemistry.[17] Surprisingly, there are only two reports concerning oxidizing intermediates from iron salen complexes.[19] Rajagopal and Ramaraj proposed a compound-I-like oxoiron(IV) salen radical from iron salen complexes and iodosylbenzene.[19a] But later Bryliakov provided spectroscopic observations against such active species and proposed the iodosylbenzene−iron(III) salen adduct.[19b] Herein, we did obtain intermediates of a higher oxidation state from iron salen complexes. And we characterized the electronic structures and investigated the reactivity of the oxidizing intermediates, to get insight into the unique reaction sequence for the nonheme iron(III) center coordinated by Tyr.

Results

Detailed Electronic Structures of Oxidizing Intermediates from 1. We investigate in detail electrochemically generated oxidizing intermediates from **1**, which is a five-coordinate monomeric iron salen complex bearing only one Cl ligand as clarified by X-ray crystallographic analysis.[18] The electrochemical behavior of **1** is investigated with cyclic voltammetry. Cyclic voltammetry of **1** does not give any clear oxidation wave at room temperature but gives two reversible oxidation waves at 233 K (Figure 2), indicating that oxidizing intermediates are stable at low temperature.

(19) (a) Sivasubramanian, V. K.; Ganesan, M.; Rajagopal, S.; Ramaraj, R. *J. Org. Chem.* **2002**, *67*, 1506−1514. (b) Bryliakov, K. P.; Talsi, E. P. *Angew. Chem., Int. Ed.* **2004**, *43*, 5228−5230.

Table 1. Oxidation Potentials of the Iron Salen Complexes[a]

compd	$E^1_{1/2}$	$E^2_{1/2}$
1	0.85	0.96
2	0.80	1.00
3	0.82	1.00
4	0.79	0.95

[a] See the caption in Figure 2 for the measurement conditions.

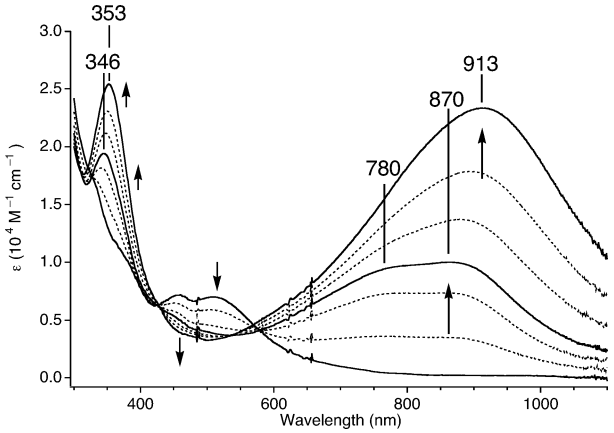

Figure 3. UV−vis spectral changes upon electrochemical oxidation of **1** in CH_2Cl_2 at 203 K. Conditions: 0.5×10^{-3} M **1**; 0.10 M tetrabutylammonium perchlorate supporting electrolyte; controlled-potential oxidation at 1.00 V for $[\mathbf{1}]^+$ and 1.30 V for $[\mathbf{1}]^{2+}$ vs Fc′/Fc. **1**, $[\mathbf{1}]^+$, and $[\mathbf{1}]^{2+}$ are depicted in a solid line.

The first ($E^1_{1/2}$) and second oxidation potential ($E^2_{1/2}$) is 0.85 and 0.96 V versus the ferrocenium/ferrocene couple, respectively (Table 1).

Consistent with the two reversible oxidation waves, a controlled-potential electrochemical oxidation of **1** at 203 K shows two-stage UV−vis spectral changes with clear isosbestic points, generating the one- and two-electron-oxidized intermediates $[\mathbf{1}]^+$ and $[\mathbf{1}]^{2+}$ as shown in Figure 3. $[\mathbf{1}]^+$ is generated through controlled-potential oxidation at 1.0 V for 2 h. An additional 2 h and an increased voltage of 1.3 V are required to generate $[\mathbf{1}]^{2+}$. The starting iron(III) complex **1** displays a characteristic phenolate-to-iron(III) charge-transfer band around 500 nm. Upon the first one-electron oxidation to $[\mathbf{1}]^+$, the intensity of this band is decreased, while an intense absorption at 346 nm and a broad absorption at 780 and 870 nm grow. The second one-electron oxidation from $[\mathbf{1}]^+$ to $[\mathbf{1}]^{2+}$, on the other hand, results in a doubled intensity and a bathochromic shift (346 to 353 nm, 780 and 870 nm to 913 nm) in these absorption maxima. These spectral changes are reversible, and the starting iron(III) complex is regenerated when the reversed potential (−0.9 V) is applied at 203 K. The intense absorption around 350 nm for $[\mathbf{1}]^+$ and $[\mathbf{1}]^{2+}$ is indicative of the phenoxyl radical formation, because phenoxyl radicals reported to date usually exhibit an absorption around 400 nm.[14,16] Chemical oxidation of **1** with tris(2,4-dibromophenyl)aminium hexachloroantimonate (**5**)[20] also generates $[\mathbf{1}]^+$ and $[\mathbf{1}]^{2+}$.[21] It was reported that phenoxyl radicals from Cu[22] and Ni salen[23]

(20) Connelly, N. G.; Geiger, W. E. *Chem. Rev.* **1996**, *96*, 877−910.
(21) $[\mathbf{1}]^+$ is generated in high yield utilizing just 1.0 equiv of the oxidant **5**, but the yield of $[\mathbf{1}]^{2+}$ is low utilizing even an excess of **5**. See Figure 5.

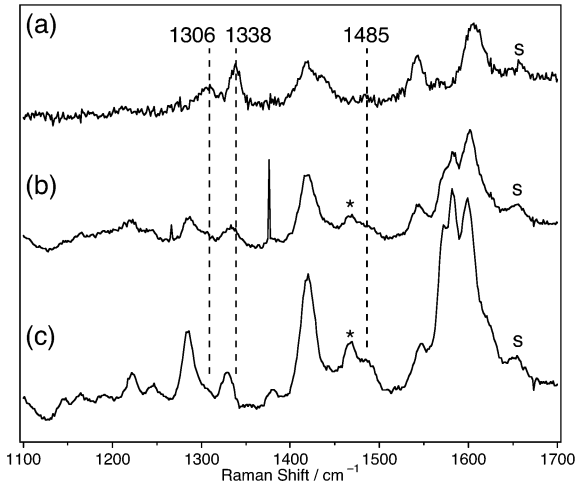

Figure 4. Resonance Raman spectra of (a) **1**, (b) **1** + 1.0 equiv of the oxidant **5**, and (c) **1** + 2.0 equiv of the oxidant **5** in CD_2Cl_2 at 193 K. The excitation wavelength is 351.4 nm. The band from CD_2Cl_2 is denoted with "s". The band designated with an asterisk is observable for the reaction product from the oxidant **5** alone in the absence of **1**. A low signal-to-noise ratio for the spectrum of **1** is due to a smaller ϵ value of **1** at 351.4 nm.

display intense absorptions (1750 and 1103 nm, respectively) in the near-infrared (NIR) region. But no additional spectral feature from 1100 to 2500 nm is observed for both $[\mathbf{1}]^+$ and $[\mathbf{1}]^{2+}$ generated by use of **5**.

To obtain more definitive evidence for the phenoxyl radical formation, resonance Raman spectra are measured at 193 K for $[\mathbf{1}]^+$ and $[\mathbf{1}]^{2+}$ generated by use of **5** in CD_2Cl_2, using an excitation wavelength of 351.4 nm. As shown in Figure 4, one of the C−O stretching band of two phenolates in **1** is observed at 1306 cm^{-1}.[18] When the 1306 cm^{-1} band is deleted by the radical formation, the nearby band at 1338 cm^{-1} is shifted to a lower frequency, indicating that the 1338 cm^{-1} mode is interacting with the C−O stretching. Upon stepwise one-electron oxidation, the 1306 cm^{-1} band exhibits decrease in intensity and instead a new band appears at 1485 cm^{-1}. The 1485 cm^{-1} band slightly increases in intensity in $[\mathbf{1}]^{2+}$ compared to $[\mathbf{1}]^+$. This band is assigned to Y7a' of the phenoxyl radical. Both 1338 and 1485 cm^{-1} bands appear as a single band, suggesting that the two phenoxyl groups have a similar structure and environment from the aspect of resonance Raman spectroscopy.

Then, Mössbauer spectra of **1**, $[\mathbf{1}]^+$, and $[\mathbf{1}]^{2+}$ dissolved in CH_2Cl_2 are measured at 11 K, to investigate the electronic state of the central iron. As shown in Figure 5 a, the iron(III) complex **1** gives a rather broad signal with an isomer shift δ of 0.21 ± 0.07 mm s^{-1} and a quadrupole splitting ΔE_Q of 0.86 ± 0.14 mm s^{-1}, indicative of high-spin iron(III).[24] Addition of 1.0 equiv of the oxidant **5** produces the spectrum shown in Figure 5b, which is fitted with two subspectra i and ii. Upon addition of 4.0 equiv of the oxidant **5**, the spectrum shown in Figure 5c is obtained. The component ii, which is a minor component in Figure 5b, is considerably increased in Figure 5c. We thus assigned the component i with δ = 0.43 ± 0.01 mm s^{-1} and ΔE_Q = 1.36 ± 0.02 mm s^{-1} to $[\mathbf{1}]^+$ and the component ii with δ = 0.31 ± 0.03 mm s^{-1} and ΔE_Q = 0.42 ± 0.06 mm s^{-1} to $[\mathbf{1}]^{2+}$.

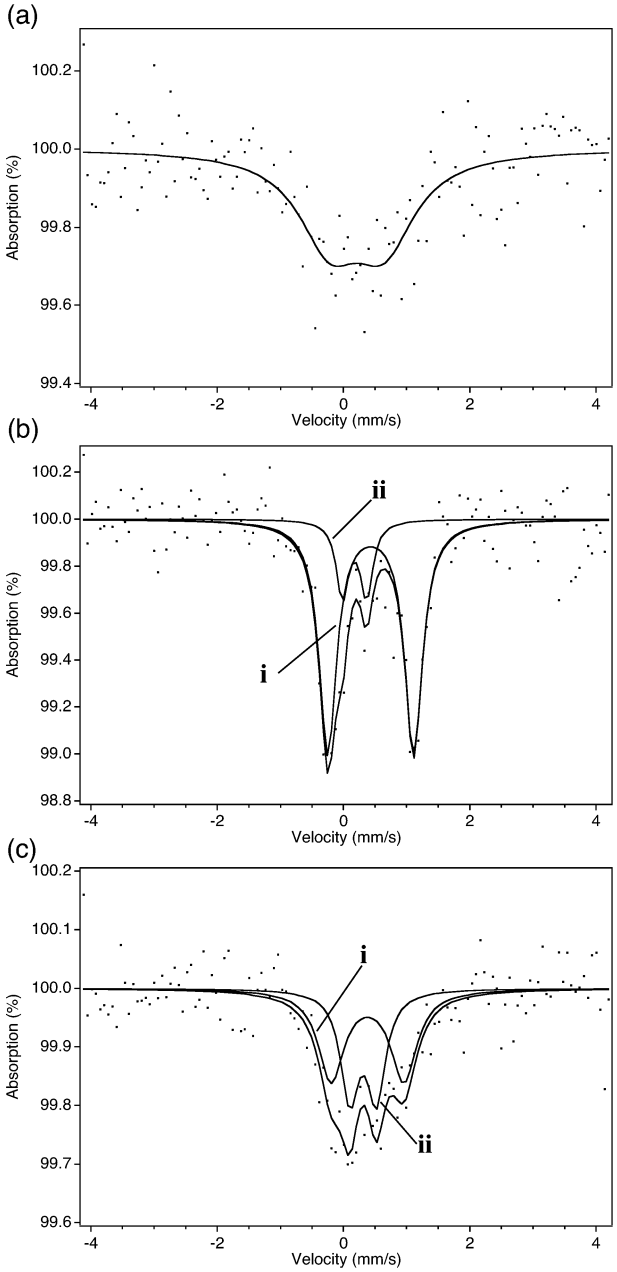

Figure 5. Zero-field Mössbauer spectra of (a) **1**, (b) **1** + 1.0 equiv of the oxidant **5**, and (c) **1** + 4.0 equiv of the oxidant **5** in CH_2Cl_2 at 11 K. The spectra in (b) and (c) were fitted with two subspectra i and ii. Mössbauer parameters: δ = 0.21 ± 0.07 mm s^{-1} and ΔE_Q = 0.86 ± 0.14 mm s^{-1} for **1**; δ = 0.43 ± 0.01 mm s^{-1} and ΔE_Q = 1.36 ± 0.02 mm s^{-1} for i; δ = 0.31 ± 0.03 mm s^{-1} and ΔE_Q = 0.42 ± 0.06 mm s^{-1} for ii.

The isomer shifts δ of 0.43 and 0.31 mm s^{-1} clearly indicate that both $[\mathbf{1}]^+$ and $[\mathbf{1}]^{2+}$ have a high-spin iron(III) center. Iron(IV) complexes reported to date usually display very small isomer shifts (0.01−0.17 mm s^{-1}).[7,25] Therefore, both the first and second one-electron oxidations are not metal-centered, indicating formation of the iron(III)−

(22) Pratt, R. C.; Stack, T. D. P. *J. Am. Chem. Soc.* **2003**, *125*, 8716−8717.
(23) Shimazaki, Y.; Tani, F.; Fukui, K.; Naruta, Y.; Yamauchi, O. *J. Am. Chem. Soc.* **2003**, *125*, 10512−10513.
(24) (a) Kennedy, B. J.; McGrath, A. C.; Murray, K. S.; Skelton, B. W.; White, A. H. *Inorg. Chem.* **1987**, *26*, 483−495. (b) Shyu, H.-L.; Wei, H.-H.; Lee, G.-H.; Wang, Y. *J. Chem. Soc., Dalton Trans.* **2000**, 915−918.

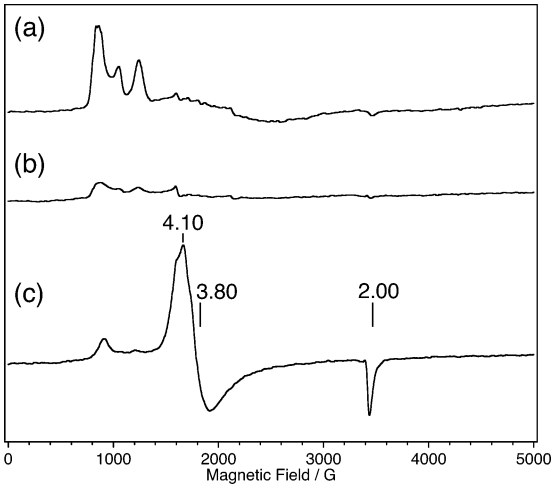

Figure 6. X-band EPR spectra of (a) **1**, (b) electrochemically generated $[\mathbf{1}]^{+}$, and (c) $[\mathbf{1}]^{2+}$ at 4 K in frozen CH_2Cl_2 containing 0.1 M tetrabutylammonium perchlorate. Conditions: microwave frequency, 9.58 GHz; microwave power, 101 μW; modulation amplitude, 7 G.

monophenoxyl and iron(III)−diphenoxyl radical complexes for $[\mathbf{1}]^{+}$ and $[\mathbf{1}]^{2+}$, respectively.

To verify the above assignment, X-band EPR spectra are recorded at 4 K for electrochemically generated $[\mathbf{1}]^{+}$ and $[\mathbf{1}]^{2+}$ as shown in Figure 6. The neutral complex **1** displays two sets of ferric high-spin signals at $g = 8.1$, 3.5, and ca. 1.8 ($E/D \approx 0.10$) and $g = 6.7$, 5.2, and ca. 2 ($E/D \approx 0.03$) in frozen CH_2Cl_2 at 4 K.[18] One-electron oxidation of **1** results in disappearance of both signals. The silent EPR signal for $[\mathbf{1}]^{+}$ is consistent with the monophenoxyl radical formation, as a result of a strong intramolecular antiferromagnetic coupling between the ferric ion ($S = 5/2$) and the phenoxyl radical ($S = 1/2$). In contrast to two species observed for **1**, $[\mathbf{1}]^{2+}$ shows one set of EPR signals at $g = 4.10$, 3.80, and 2.00, typical of $S_t = 3/2$ ($E/D \approx 0.02$). The observed $S_t = 3/2$ spin system is well accounted for by the diphenoxyl radical formation, considering an antiferromagnetic coupling between the ferric ion ($S = 5/2$) and the two phenoxyl radicals ($S = 1/2$) on the salen ligand.

To establish the chemical structures for $[\mathbf{1}]^{+}$ and $[\mathbf{1}]^{2+}$, ESI mass spectra are measured at low temperature in a positive mode. The solution of $[\mathbf{1}]^{+}$ generated by 1.2 equiv of **5** gives a single signal at *m*/*z* 1065.47 as a singly charged ion (Figure 7a). The solution of $[\mathbf{1}]^{2+}$ generated by 4.0 equiv of **5** produces predominantly a signal at *m*/*z* 532.71 as a doubly charged ion (Figure 7b). These results are consistent with formation of $[Fe(salen)Cl]^{+}$ and $[Fe(salen)Cl]^{2+}$, in which one and two electrons are removed from the starting **1**, with no concomitant chemical reaction (Figure 7c,d).

Effect of the Fifth Ligand. The fifth ligand could considerably influence the electronic state and the geometry of the resting iron(III) center. Then, the iron salen complexes bearing H_2O (**2**) and EtO (**3**) are investigated. We also

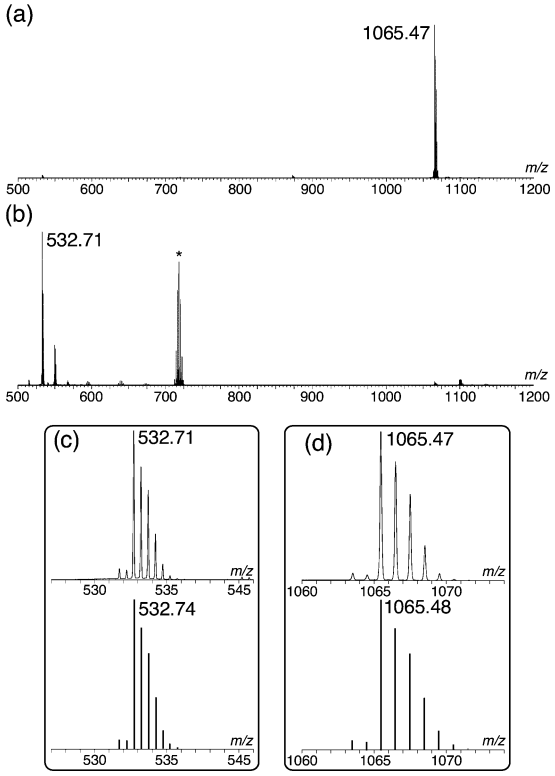

Figure 7. ESI mass spectra of (a) **1** + 1.2 equiv of the oxidant **5** and (b) **1** + 4.0 equiv of the oxidant **5** in CH_2Cl_2. The signal denoted with an asterisk comes from the oxidant **5**. (c, d) Observed (top) and calculated (bottom) isotope distribution patterns. Calculations are done for (c) [**1**, $C_{70}H_{74}ClFeN_2O_2]^{2+}$ and (d) [**1**, $C_{70}H_{74}ClFeN_2O_2]^{+}$.

explore a possibility of a high-valent iron−oxo formation from the OH complex **4**, following the successful examples in the heme chemistry.[26]

Cyclic voltammograms are measured for **2** and **3** under exactly the same experimental conditions for **1**. Closely similar to **1**, both **2** and **3** exhibit two reversible oxidation waves. The $E^1_{1/2}$ and $E^2_{1/2}$ values are almost identical with those of **1** (0.80 and 1.00 V for **2**, 0.82 and 1.00 V for **3**) as shown in Table 1.

Electrochemical oxidation of **2** in CH_2Cl_2 at 203 K successfully generates $[\mathbf{2}]^{+}$ and $[\mathbf{2}]^{2+}$ as shown in Figure 8. In the case of **2**, chemical oxidation by **5** cannot be employed, because the H_2O ligand is easily replaced with Cl ions in **5**.[20] Formation of phenoxyl radicals similar to **1** is evident from the characteristic absorption around 350 and 850−900 nm, compared to the spectra in Figure 3. EPR further supports formation of the monophenoxyl radical for $[\mathbf{2}]^{+}$ and the diphenoxyl radical for $[\mathbf{2}]^{2+}$ (Figure 9). One-electron oxidation of **2** results in disappearance of the ferric signal from **2**, just in the same way as **1**. The following one-electron oxidation produces a $S_t = 3/2$ EPR signal with $g = 4.30$, 3.58, and 1.98 ($E/D \approx 0.07$). It is interesting to note that

(25) (a) Collins, T. J.; Kostka, K. L.; Münck, E.; Uffelman, E. S. *J. Am. Chem. Soc.* **1990**, *112*, 5637−5639. (b) Collins, T. J.; Fox, B. G.; Hu, Z. G.; Kostka, K. L.; Münck, E.; Rickard C. E. F.; Wright, L. J. *J. Am. Chem. Soc.* **1992**, *114*, 8724−8725. (c) Kostka, K. L.; Fox, B. G.; Hendrich, M. P.; Collins, T. J.; Rickard C. E. F.; Wright, L. J. Münck, E. *J. Am. Chem. Soc.* **1993**, *115*, 6746−6757.

(26) (a) Lee, W. A.; Calderwood, T. S.; Bruice, T. C. *Proc. Natl. Acad. Sci. U.S.A.* **1985**, *82*, 4301−4305. (b) Calderwood, T. S.; Lee, W. A.; Bruice, T. C. *J. Am. Chem. Soc.* **1985**, *107*, 8272−8273. (c) Groves, J. T.; Gilbert, J. A. *Inorg. Chem.* **1986**, *25*, 123−125. (d) Calderwood, T. S.; Bruice, T. C. *Inorg. Chem.* **1986**, *25*, 3722−3724. (e) Swistak, C.; Mu, X. H.; Kadish, K. M. *Inorg. Chem.* **1987**, *26*, 4360−4366. (f) Groves, J. T.; Gross, Z.; Stern, M. K. *Inorg. Chem.* **1994**, *33*, 5065−5072.

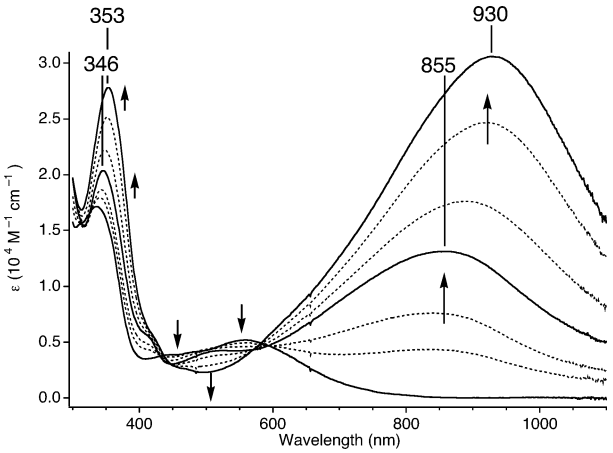

Figure 8. UV−vis spectral changes upon electrochemical oxidation of **2** in CH_2Cl_2 at 203 K. Conditions: 0.5×10^{-3} M **2**; 0.10 M tetrabutylammonium perchlorate supporting electrolyte; controlled-potential oxidation at 1.00 V for $[\mathbf{2}]^+$ and 1.30 V for $[\mathbf{2}]^{2+}$ vs Fc′/Fc. **2**, $[\mathbf{2}]^+$, and $[\mathbf{2}]^{2+}$ are depicted in a solid line.

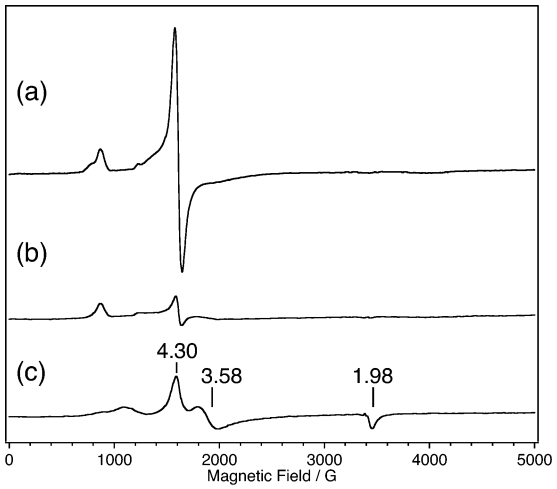

Figure 9. X-band EPR spectra of (a) **2**, (b) electrochemically generated $[\mathbf{2}]^+$, and (c) $[\mathbf{2}]^{2+}$ at 4 K in frozen CH_2Cl_2 containing 0.1 M tetrabutylammonium perchlorate. Conditions: microwave frequency, 9.58 GHz; microwave power, 101 μW; modulation amplitude, 7 G.

$[\mathbf{2}]^{2+}$ ($E/D \approx 0.07$) is more rhombic than the $[\mathbf{1}]^{2+}$ ($E/D \approx 0.02$), while the neutral complex **2** ($E/D \approx 0.21$) has also a more rhombic iron center than **1** ($E/D \approx 0.03$, 0.10).

In contrast to **1** and **2**, a UV−vis spectral change upon electrochemical oxidation of **3** shows no isosbestic points, indicative of more than two oxidation pathways. Upon addition of 5% of EtOH to the CH_2Cl_2 solution of **3**, one of these pathways seems to prevail as suggested by the clear isosbestic points (Figure 10). However, the spectral change is distinctively different from those of **1** and **2**. The absorption at 350 and 530 nm is increased, while the absorption at 410 nm is decreased. The resulting spectrum, which is rather close to that of the aqua complex **2**, is not affected at all upon the reversed-potential electrochemical oxidation (−0.9 V) at 203 K, suggesting that the coordinated EtO group is oxidized upon one-electron oxidation. Then, the EtO group is replaced with the CD_3O group, which is more resistant to oxidation. But the UV−vis spectral change is exactly the same, suggesting that even the CD_3O group is

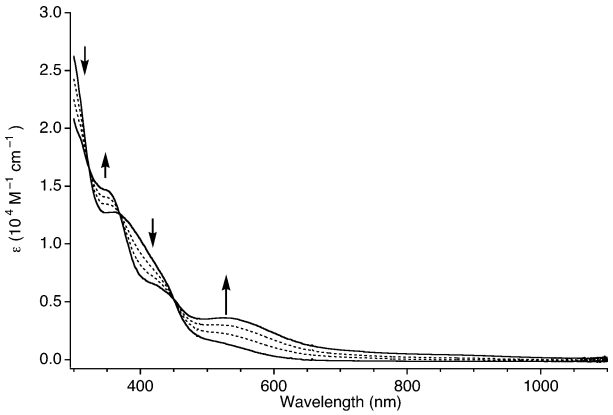

Figure 10. UV−vis spectral changes upon electrochemical oxidation of **3** in CH_2Cl_2−EtOH (95:5) at 203 K. Conditions: 0.5×10^{-3} M **3**; 0.10 M tetrabutylammonium perchlorate supporting electrolyte; controlled-potential oxidation at 0.83 V vs Fc′/Fc.

oxidized. An EPR measurement is consistent with this interpretation, and the ferric high-spin signal remains intact in intensity after the irreversible one-electron oxidation. As expected, quantitative analysis of the resulting solution after controlled-potential oxidation of **3** shows generation of acetaldehyde in ca. 25% net yield. Notably, the present iron salen complex exhibits a considerably high reactivity for the coordinated alcohol.

To examine the reactivity of $[\mathbf{2}]^+$, 2 equiv of benzyl alcohol is introduced at 203 K to the solution of the electrochemically generated $[\mathbf{2}]^+$. Surprisingly, the UV−vis spectrum of $[\mathbf{2}]^+$ remains intact, and benzyl alcohol is not oxidized. However, upon addition of 2,6-di-*tert*-butylpyridine, the characteristic UV−vis spectrum of $[\mathbf{2}]^+$ is diminished very quickly. Indeed, analysis of the resulting solution with GC-MS shows formation of benzaldehyde in 56 ± 2% yield. Considering the high reactivity for EtO group upon one-electron oxidation of **3**, a base to remove a proton from alcohol OH is required to initiate oxidation sequences from alcohol to aldehyde. Reactivity of $[\mathbf{2}]^{2+}$ is investigated in the same manner, but the yield of benzaldehyde is not changed at all (57 ± 5%), indicating that the one-electron oxidized state from the iron(III) complex is enough for oxidation of alcohols. Reaction with cyclohexene is also examined, but cyclohexene oxide, 2-cyclohexene-1-ol, and 2-cyclohexene-1-one are not detected at all (<0.5%).

The OH complex **4** is produced by addition of tetrabutylammonium hydroxide to the CH_2Cl_2 solution of **2** through acid−base equilibrium but under an excess of tetrabutylammonium hydroxide (2.5 equiv). Cyclic voltammetry of **4** gives two reversible oxidation waves at 0.79 and 0.95 V (Table 1), with an additional broad irreversible oxidation wave around 0.45 V, which is assigned to oxidation of tetrabutylammonium hydroxide. Upon electrochemical oxidation of **4**, the UV−vis spectral change follows acid−base equilibrium back to **2**, probably due to oxidation of an excess of tetrabutylammonium hydroxide. The further oxidation of the resulting solution then generates an EPR-silent species, which is an iron(III)−phenoxyl radical, judging from the characteristic UV−vis spectrum at λ ($\epsilon/10^4$ M^{-1} cm^{-1}) = 345 (1.87) and 850 (0.94) nm.

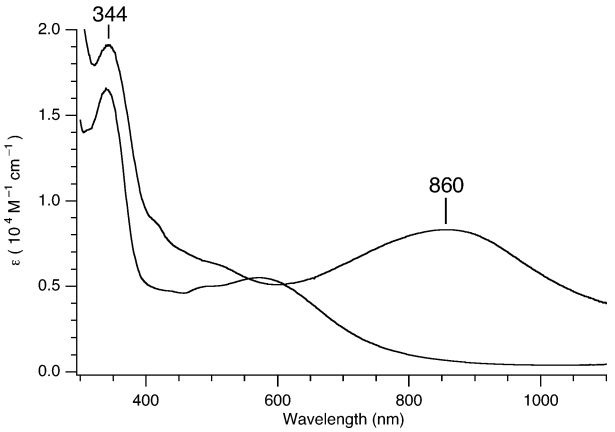

Figure 11. UV−vis spectra of **2** and **2** + 1 equiv of *m*CPBA in CH_2Cl_2 at 193 K. Conditions: 1.5×10^{-4} M **1**; 1.5×10^{-4} M *m*CPBA.

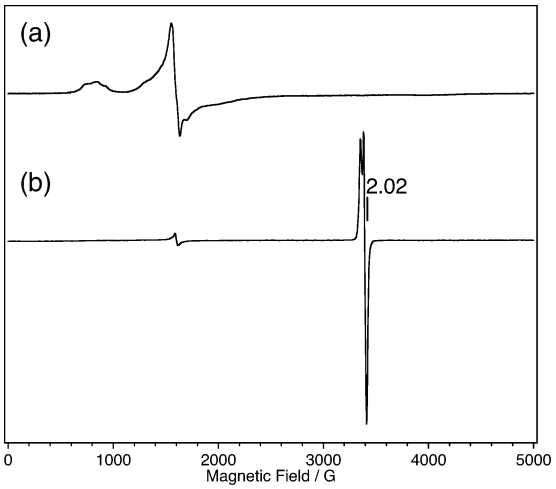

Figure 12. X-band EPR spectra of (a) **2** and (b) **2** + 3 equiv of *m*CPBA at 1.6 K in frozen toluene−CH_2Cl_2 (3:7). Conditions: microwave frequency, 9.59 GHz; microwave power, 101 μW; modulation amplitude, 7 G.

Oxidizing Intermediates from the Iron Salen Complex and *m*CPBA. With the fully characterized iron(III)−phenoxyl radical from the iron salen complex on hand, we then investigate oxidizing intermediates generated by *m*CPBA, which has been frequently utilized to generate high-valent metal−oxo species in the porphyrin chemistry.[17] Addition of 1 equiv of *m*CPBA to the CH_2Cl_2 solution of **2** generates a blue-green solution with absorption maxima at 344 and 860 nm shown in Figure 11. Titration of **2** with *m*CPBA shows a saturation behavior, and the absorption at 344 and 860 nm does not increase any more upon addition of more than ca. 0.8 equiv of *m*CPBA. Compared to the UV−vis spectra for $[\mathbf{1}]^+$ and $[\mathbf{1}]^{2+}$ in Figure 3, the absorption at 344 and 860 nm is indicative of the monophenoxyl radical formation on the salen ligand. Indeed, using an excitation wavelength at 413.1 nm, a broad resonance Raman band appears at 1485 cm^{-1}, exactly the same wavenumber as $[\mathbf{1}]^+$. An EPR measurement also supports the monophenoxyl radical formation around the iron(III) center. The ferric high-spin signal for **2** disappears in the blue-green solution (Figure 12). An additional feature is observed at $g \approx 2$, but the origin of this signal is not identified. Stoichiometry of *m*CPBA to the monophenoxyl radical formation is roughly evaluated using the $\epsilon_{855\ nm}$ value for $[\mathbf{2}]^+$ (13 100 M^{-1} cm^{-1}). With utilization of a large excess of **2** (20 equiv), 1 equiv of *m*CPBA generates 2 equiv of the monophenoxyl radical, suggesting that all the oxidizing equivalents from *m*CPBA are retained in the blue-green solution.

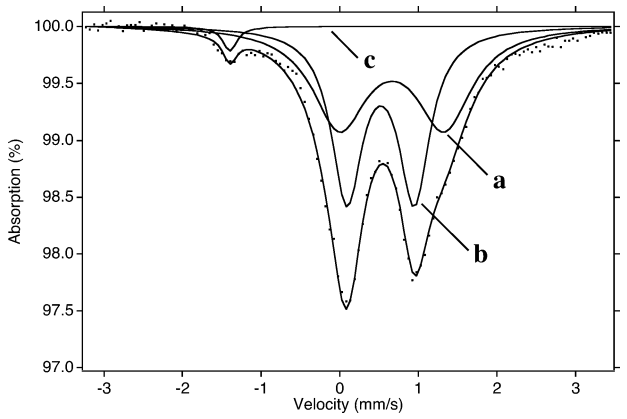

Figure 13. Zero-field Mössbauer spectra of **2** + 3 eqiuv of *m*CPBA in toluene−CH_2Cl_2 (3:7) at 5 K. The spectrum was fitted with three subspectra **a**−**c**. Mössbauer parameters: $\delta = 0.66 \pm 0.01$ mm s^{-1} and $\Delta E_Q = 1.33 \pm 0.04$ mm s^{-1} for **a**; $\delta = 0.52 \pm 0.06$ mm s^{-1} and $\Delta E_Q = 0.86 \pm 0.01$ mm s^{-1} for **b**. For **c**, the Mössbauer parameters could not be determined.

The Mössbauer spectrum, on the other hand, indicates that the blue-green solution contains equimolar amounts of the components **a** and **b** as shown in Figure 13. The component **a** is fitted with $\delta = 0.66 \pm 0.01$ mm s^{-1} and $\Delta E_Q = 1.33 \pm 0.04$ mm s^{-1}, and the component **b** is fitted with $\delta = 0.52 \pm 0.06$ mm s^{-1} and $\Delta E_Q = 0.86 \pm 0.01$ mm s^{-1}. In addition, a trace amount of the component **c** is observed, but the Mössbauer parameters could not be determined. As indicated by the δ values, both the component **a** and **b** contain an iron(III) center. The ΔE_Q value for the component **a** is almost identical with that for $[\mathbf{1}]^+$, supporting formation of the monophenoxyl radical. But the ΔE_Q value for the component **b** is rather small.

To get insight into the fifth ligand of oxidizing intermediates in the blue-green solution, the ESI mass spectrum is measured at low temperature in a positive mode. The CH_2Cl_2 solution of **2** gives a single signal at *m*/*z* 1030.51 as a singly charged ion, which corresponds to $[Fe^{III}(salen)]^+$ with loss of H_2O and ClO_4^- from **2**. The blue-green solution generated from **2** and 3 equiv of *m*CPBA gives a predominant signal at *m*/*z* 1046.43 as a singly charged ion. The mass value of *m*/*z* 1046.43 is increased by 16 Da from $[Fe^{III}(salen)]^+$. By use of the ^{18}O-labeled *m*CPBA, this signal is shifted by 2.0 Da, indicating that the predominant species detected with a mass spectrometer is $[Fe(salen)O]^+$ and that the oxygen atom comes from *m*CPBA. Reduction of the blue-green solution with ferrocene results in complete disappearance of the signal at *m*/*z* 1046.43. Instead, the signal at *m*/*z* 1030.64 is regenerated, together with an unidentified signal at *m*/*z* 1231.67, indicating that the signal at *m*/*z* 1046.43 arises from a transient intermediate and not from a ligand-oxidation product.

Discussion

Phenoxyl Radicals from the Iron Salen Complex. Oxidizing intermediates generated through stepwise one-

electron oxidation of the iron(III) salen complex is subjected to a thorough spectroscopic investigation. The N_2O_2 coordination environment of the salen ligand is indeed found for the active site in nonheme iron(III) enzymes, such as 3,4-PCD.[11] In addition, the metal salen complex is one of the most important catalysts in synthetic chemistry.[27] Therefore, the electronic structure of oxidizing intermediates from the iron salen complex assumes a fundamental importance, not only from a bioinorganic aspect but also from a design of effective oxidation catalysts.

Stepwise one-electron oxidation of **1** bearing Cl as a fifth ligand generates the one- and two-electron-oxidized intermediates $[\mathbf{1}]^+$ and $[\mathbf{1}]^{2+}$, having an intense absorption around 350 nm and a characteristic broad absorption around 500−1100 nm. This study clearly indicates that $[\mathbf{1}]^+$ and $[\mathbf{1}]^{2+}$ are best represented as the mono- and diphenoxyl radicals coordinated to the iron(III) center, respectively. It is not trivial to determine oxidation states of iron centers only from Mössbauer parameters, when noninnocent ligands are coordinated to the iron center, as discussed recently by Walker and Trautwein.[28] But in the present case isomer shifts δ for both $[\mathbf{1}]^+$ and $[\mathbf{1}]^{2+}$ are rather increased from the starting iron(III) complex **1**, indicating that the iron center in both $[\mathbf{1}]^+$ and $[\mathbf{1}]^{2+}$ bears iron(III) character. In addition, the phenoxyl radical formation on the salen ligand is suggested by the intense absorption around 350 nm. Indeed, resonance Raman measurements upon excitation at 351.4 nm give a resonance Raman band around 1485 cm^{-1}, which could be assigned to the phenoxyl radical C−O stretching.

The complex **1** shows two sets of EPR signals from high-spin iron(III) centers in frozen CH_2Cl_2 at 4 K, major component with $g = 8.1$, 3.5, and ca. 1.8 ($E/D \approx 0.10$) and minor component with $g = 6.7$, 5.2, and ca. 2 ($E/D \approx 0.03$). This suggests that two iron(III) species of different rhombicity are present in solution. The EPR parameter of the major component is close to that of the previous report.[19b] On the other hand, we assigned the minor component to a six-coordinated form resulting from binding of ethanol to **1** in our previous paper,[18] but this species is still present when EPR spectra are measured in amylene-stabilized CH_2Cl_2 for the well-dried **1**. We thus reinterpret that **1** in a five-coordinated form may have a metastable structure due to steric repulsion from mesityl groups. In frozen solution, the stable structure, which has been shown by the X-ray crystal structure, would provide the EPR signals for the major component and the metastable structure would be the EPR signals for the minor component. On the other hand, ^{1}H NMR in CD_2Cl_2 at 193 K shows only one set of signals for the phenolate rings, indicating that these two species are interconverted with each other very fast compared to the NMR time scale. Upon stepwise one-electron oxidation, both species are oxidized in the same manner as indicated by EPR. In contrast to **1**, $[\mathbf{1}]^{2+}$ exhibits only one set of a $S = 3/2$ signal, suggesting that one of the species is converted to the other upon stepwise one-electron oxidation.

The phenoxyl radical complexes from **1** display a $\pi \rightarrow \pi^*$ transition of the phenoxyl radical at $\lambda_{max} \approx 346$ nm, which is largely shifted from the reported values of 400 ± 20 nm for phenoxyl radicals.[13,14,16] The observed hypsochromic shift is probably due to introduction of the electron-withdrawing imino groups to the ortho position of the phenolate ring, causing a consierable energy lowering of the HOMO level. Indeed, **1** exhibits a considerably high oxidation potential ($E^1_{1/2} = 0.85$ V), compared to other examples such as the Wieghardt's macrocylic iron(III) complex ($E^1_{1/2} = 0.11$ V).[14c] The other characteristic feature in the UV−vis spectra of the present phenoxyl radical is an intense broad absorption around 500−1100 nm ($\epsilon = 10\,000$, $23\,000$ M^{-1} cm^{-1} for $[\mathbf{1}]^+$ and $[\mathbf{1}]^{2+}$, respectively). The best assignment for this absorption feature is the charge transfer between the iron(III) center and the phenoxyl radical, because $[\mathbf{1}]^{2+}$, in which all the two phenolates are converted to the phenoxyls, displays the broad absorption of a doubled intensity in this region, compared to $[\mathbf{1}]^+$ bearing one phenolate and one phenoxyl.

Quite interestingly, the active form of galactose oxidase (GO) does exhibit a similar feature ($\epsilon = \sim 5000$ M^{-1} cm^{-1}) around 600−1200 nm, but Whittaker and Spiro proposed that this feature arises from a interligand charge transfer from the tyrosinate to the thiolate-modified tyrosyl radical.[29] Synthetic phenoxyl radicals from the Cu and Ni salen complexes were reported to show a NIR absorption feature at 1750 nm ($\epsilon = 2400$ M^{-1} cm^{-1})[22] and 1103 nm ($\epsilon = 3000$ M^{-1} cm^{-1}),[23] respectively. In the case of the Cu salen, the absorption at 1750 nm is assigned to the phenolate−phenoxyl charge transfer. But $[\mathbf{1}]^+$ exhibits no additional absorption in the NIR region from 1100 to 2500 nm, indicating that the phenolate−phenoxyl charge-transfer absorption in $[\mathbf{1}]^+$ is not present or hidden behind the intense absorption around 500−1100 nm. Considering that **1** has two distinct phenolate rings due to the distortion,[18] the phenolate−phenoxyl charge-transfer absorption in $[\mathbf{1}]^+$ is possibly shifted to higher energy, compared to the nondistorted Cu salen bearing two phenolate rings of a similar environment. The absorption feature around 780 nm in $[\mathbf{1}]^+$ might be a candidate, because this feature disappears in $[\mathbf{1}]^{2+}$.

It is also interesting to note that a quadrupole splitting ΔE_Q is much larger for $[\mathbf{1}]^+$ (1.36 mm s^{-1}) than **1** (0.86 mm s^{-1}). The ΔE_Q value of 0.86 mm s^{-1} for **1** clearly indicates high-spin iron(III), because low-spin iron(III) salen complexes exhibit larger ΔE_Q value (>2 mm s^{-1}).[24] The larger ΔE_Q is indicative of lower symmetry around the iron center. In the previous report by Koikawa et al. on one-electron oxidation of a similar iron(III)−phenolate system, a large ΔE_Q is ascribed to the iron(IV) formation.[30] However, as already pointed out by Wieghardt,[13,14] a large ΔE_Q for iron(III)−phenolate systems is rather consistent with the

(27) McGarrigle, E. M.; Gilheany, D. G. *Chem. Rev.* **2005**, *105*, 1563−1602.
(28) Zakharieva, O.; Schünemann, V.; Gerdan, M.; Licoccia, S.; Cai, S.; Walker, F. A.; Trautwein, A. X. *J.* Am. *Chem. Soc.* **2002**, *124*, 6636−6648.
(29) McGlashen, M. L.; Eads, D. D.; Spiro, T. G.; Whittaker, J. W. *J. Phys. Chem.* **1995**, *99*, 4918−4922.
(30) Koikawa, M.; Okawa, H.; Maeda, Y.; Kida, S. *Inorg. Chim. Acta* **1992**, *194*, 75−79.

phenoxyl radical formation, when it is assumed that the radical is localized to one of the phenolate rings of the salen ligand on the Mössbauer time scale, leading to an electronically unsymmetrical environment. Our study provides further support for the interpretation on the ΔE_Q value, because oxidation of both phenolate rings on the salen ligand, generating more symmetrical environment than $[\mathbf{1}]^+$, indeed results in the smaller ΔE_Q value for $[\mathbf{1}]^{2+}$ (0.42 mm s^{-1}).

Vacant Coordination Site on the Iron Salen Complex. A fifth ligand on the vacant coordination site could be an important factor to determine the electronic state and the geometry of the resting iron(III) center. The effect of a fifth coordination ligand is worth discussing here, because previous iron(III)−phenoxyl radical complexes have no vacant coordination site on the iron(III) center. From this viewpoint, particularly interesting for the present model system is a drastic structural change upon exchange of the fifth ligand from Cl (**1**) to OH_2 (**2**).[18] As revealed by X-ray crystallographic analysis, the ferric aqua complex **2** displays a distorted trigonal-bipyramidal iron(III) center, while the structure of **1** is rather close to the common square-pyramidal. Such a structural difference is seemingly retained in solution, because EPR measurements indicate that **2** ($E/D \approx 0.21$) has a much more rhombic iron center than **1** ($E/D \approx 0.03, 0.10$). However, the structural difference around the iron center does not exert any observable influence on the electrochemical behavior of **1** and **2**, and both **1** and **2** generate the iron(III)−phenoxyl radical complex upon electrochemical oxidation. Quite interestingly, the structural distortion caused by the coordination of H_2O is retained in the oxidized form of **2**, because $[\mathbf{2}]^{2+}$ ($E/D \approx 0.07$) is also more rhombic than $[\mathbf{1}]^{2+}$ ($E/D \approx 0.02$)

The present model system is the first example of the iron(III)−phenoxyl radical complex bearing the vacant coordination site and, thus, provides an opportunity to examine reactivity relevant to iron enzymes having the phenolate group coordinated to the iron(III) center. Particularly remarkable is one-electron oxidation of the EtO or CD_3O complexes causes conversion of alcoxide to aldehyde even at low temperature. The iron(III) porphyrin cation radical does not have such reactivity at all, but coordination of the electron-donating CH_3O groups results in formation of a rather stable iron(IV) intermediate.[31] One of interesting findings from a mechanistic perspective is a clear demonstration of necessity of a base to remove an alcohol proton. As already described, both $[\mathbf{2}]^+$ and $[\mathbf{2}]^{2+}$ do not oxidize even benzyl alcohol at all, unless 2,6-di-*tert*-butylpyridine is added to the solution. Once benzyl alcohol is converted to alcoxide on the iron(III) center, conversion to benzaldehyde proceeds smoothly without a base, as suggested by oxidation of EtO in **3**. Another point to be noted is that a negligible difference is observed for reactivity of $[\mathbf{2}]^+$ and $[\mathbf{2}]^{2+}$, indicating that the monophenoxyl radical complex is the key intermediate for oxidation of alcohols and that one more oxidizing equivalent does not contribute to effectiveness. This might be due to very fast reduction of $[\mathbf{2}]^{2+}$ to $[\mathbf{2}]^+$ before reaction with benzyl alcohol upon addition of 2,6-di-*tert*-butylpyridine. High reactivity of the present iron(III)−phenoxyl radical for alcohols may imply that the copper ion in the active site of GO could be replaced with other metals, just when the metal center binds a substrate in close vicinity to the phenoxyl radical and also functions as a Lewis acid. Indeed, phenoxyl radical complexes with other metals such as zinc and alkaline earth metal ions have already been reported to exhibit oxidation reactivity.[16d,e,32]

Scheme 1

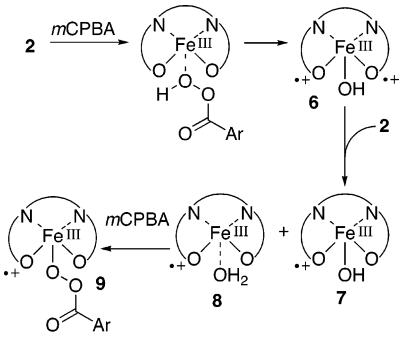

In contrast to the oxoiron(IV) formation from the hydroxoiron(III) porphyrin upon one-electron oxidation, the iron salen complex **4** bearing OH does not generate a high-valent iron species. Upon the initial stage of electrochemical oxidation, the fifth OH ligand in **4**, which is retained under an excess of tetrabutylammonium hydroxide, is supposed to be protonated to a considerable extent due to oxidation of an excess of tetrabutylammonium hydroxide. This is supported by the UV−vis spectral change, which suggests that an acid−base equilibrium is considerably shifted from **4** to **2**. Further oxidation generates an iron(III)−phenoxyl radical, but the fifth ligand is not pure OH.

Oxidizing Intermediates from the Iron Salen Complex and *m*CPBA. In the case of the heme chemistry, a model intermediate relevant to the oxygen activation by heme enzymes was first synthesized from the iron(III) porphyrin complex and *m*CPBA and was identified to be the oxoiron(IV) porphyrin π-cation radical by Groves.[17a] On the other hand, reaction of **2** with *m*CPBA at 193 K generates the blue-green solution whose UV−vis spectrum is closely similar to the iron(III)−monophenoxyl radicals such as $[\mathbf{1}]^+$ and $[\mathbf{2}]^+$. The EPR spectrum further supports the monophenoxyl radical formation, because the ferric high-spin signal for **2** disappears in the blue-green solution. But the Mössbauer spectrum reveals that the blue-green solution contains two iron(III) intermediates of an equimolar amount.

We postulate the reaction sequence shown in Scheme 1, based on the experimental observation that all the oxidizing equivalents are retained in the blue-green solution. Reaction of **2** with *m*CPBA gives a two-electron-oxidized intermediate **6** at first. But **6** is readily reduced by another molecule of **2** to give two molecules of monophenoxyl radicals **7** and **8**. This accounts well for the saturation behavior by addition of less than 1 equiv of *m*CPBA. An excess of *m*CPBA

(31) Groves, J. T.; Quinn, R.; McMurry T. J.; Nakamura, M.; Lang, G.; Boso, B. *J. Am. Chem. Soc.* **1985**, *107*, 354−360.

(32) Itoh, S.; Kumei, H.; Nagatomo, S.; Kitagawa, T.; Fukuzumi, S. *J. Am. Chem. Soc.* **2001**, *123*, 2165−2175.

converts **8** to **9** by exchange of the fifth ligand from H_2O to *m*-chloroperoxybenzoate.

Among two major components observed in the Mössbauer spectrum, the component **a** with $\delta = 0.66$ mm s^{-1} and $\Delta E_Q = 1.33$ mm s^{-1} would correspond to **7**, because the ΔE_Q value, which is almost identical with that for $[\mathbf{1}]^+$, indicates the unsymmetrical monophenoxyl radical. The larger isomer shift δ of 0.66 mm s^{-1} compared to $[\mathbf{1}]^+$ could be explained by coordination of the more electron-donating ligand OH as a fifth ligand. We tentatively assign the component **b** with $\delta = 0.52$ mm s^{-1} and $\Delta E_Q = 0.86$ mm s^{-1} to **9**. The smaller ΔE_Q value might be due to an electron-accepting nature of the *m*-chloroperoxybenzoate ligand to increase symmetry around the iron(III) center. ESI mass spectrometry supports the above scenario, and the signal at *m*/*z* 1046.43 could be considered to originate from **9** through a homolytic cleavage of the weak O−O bond during an ionization process. This signal apparently matches the oxoiron(IV) salen phenoxyl radical complex or the oxoiron(V) salen complex, but the presence of such species in solution is denied by the other spectroscopic data.

Implications. We employ two independent routes to the nonheme high-valent iron−oxo intermediate from the iron salen complex, electrochemical oxidation of the OH complex **4** and *m*CPBA oxidation of **2**, both of which are the established pathways to the high-valent metal−oxo species in the porphyrin chemistry. Unexpectedly, both routes lead to generation of very unstable iron(III)−phenoxyl radicals, although the salen ligand is harder to be oxidized than the porphyrin ligand bearing the large π-conjugation. It is also in sharp contrast to the heme chemistry that electrochemical oxidation of **3** bearing an electron-donating EtO ligand results in oxidative degradation of the EtO group and not in the iron(IV) formation. These results indicate that the phenolate (Tyr) coordination to the iron(III) center brings about a considerable preference for the iron(III) state over the iron(IV), irrespective of a high oxidation potential of the surrounding coordination environment.

A bunch of mononuclear nonheme iron(II) enzymes, which share the common His_2Asp/Glu motif around the iron(II) center referred to as the 2-His-1-carboxylate facial triad, are proposed to employ similar mechanistic strategies with heme enzymes in oxidation catalysis.[33] Indeed, a compound-II-like oxoiron(IV) intermediate was detected in the oxidation cycle by TauD, a mononuclear nonheme iron enzyme of this category.[6] Furthermore, several iron(II) model complexes bearing the similar nitrogen coordination environment were demonstrated to generate an oxoiron(IV) species,[7] suggesting that the His-coordinated iron(II) center utilizes an oxoiron(IV) species to effect oxidation reactions. On the other hand, a mechanistic scenario seems to be utterly different for mononuclear iron(III) enzymes with the His_2Tyr_2 motif around the iron(III) center, such as 3,4-PCD. As clarified in this manuscript, the phenolate-coordinated iron(III) center sticks to the iron(III) state and, therefore, follows a reaction pathway mechanistically distinct from the heme paradigm. A considerably high reactivity for coordinated substrate on the iron(III) center might be a hint to understand a rather unique reaction sequence upon oxygen activation.

Finally, we describe another important implication for this study. The salen ligand is one of the most successful frameworks for development of effective transition metal catalysts, but disappointedly low reactivity has been repeatedly encountered for the iron metal. The poor catalytic activity for epoxidation compared to Mn and Cr salens can be now understood very well by a considerable preference for the iron(III) state in the salen framework. By analogy to the heme chemistry, the iron salen complex has been elucidated to give a compound I analogue as a reactive intermediate, but this might be not true for most iron salen complexes in light of the present comprehensive investigation. Recently, Rajagopal and Ramaraj reported a mechanistic study on oxygenation of organic sulfides by iron salen complexes.[19a] They elucidated the oxoiron(IV) salen radical formation from several iron salen complexes and PhIO on the basis of limited spectroscopic data and discussed the oxygenation mechanism. But we have to point out that their mechanistic elucidation remains to be investigated.

Conclusion

The model complex for mononuclear iron(III) enzymes, bearing two His and two Tyr coordinated to the iron(III) center, is investigated in detail to reveal the relationship between the electronic structure and the reactivity of oxidizing intermediates. The model complex employed in this study is the sterically hindered iron salen complex, which well reproduces a coordination environment by His_2Tyr_2 and most importantly a vacant coordination site on the iron(III) center. In contrast to the oxoiron(IV) formation from heme models and His-coordinated nonheme iron(II) centers, the iron salen complex generates the iron(III)−phenoxyl radical irrespective of the fifth ligand. The nonheme iron center coordinated with the phenolate group is resistant to adopt the iron(IV) state even in a highly oxidizing environment. The vacant coordination site also enables investigations on reactivity, which reveals a highly oxidizing nature of the iron(III)−phenoxyl for coordinated alcohols. This study explains unique properties of mononuclear nonheme enzymes with Tyr residues and also the poor epoxidation activity of Fe salen compared to Mn and Cr salens.

Experimental Section

Instrumentation. Cyclic voltammograms were measured with a ALS612A electrochemical analyzer (BAS). UV−vis spectra were recorded on an Agilent 8453 (Agilent Technologies) equipped with a USP-203 low-temperature chamber (UNISOKU). UV−vis spectra in the NIR region were measured with Hitachi U-3500. EPR spectra were recorded in a quartz cell ($d = 5$ mm) at 4 K on an E500 continuous-wave X-band spectrometer (Bruker) with an ESR910 helium-flow cryostat (Oxford Instruments). Resonance Raman spectra were measured with a quartz spinning cell kept at 193 K, using a MC-100DG 100-cm single polychromator (Ritsu Ohyo Kogaku) equipped with a LN/CCD-1100-PB liquid- nitrogen-cooled CCD detector (ROPER Scientific). A BeamLok 2080 argon ion

(33) Hegg, E. L.; Que, L., Jr. *Eur. J. Biochem.* **1997**, *250*, 625−629.

laser (Spectra Physics) was utilized as an excitation source. The laser power at the sample was about 10 mW. Raman shifts were calibrated with indene. ESI mass spectra were obtained with a LCT time-of-flight mass spectrometer equipped with an electrospray ionization interface (Micromass).

Materials. CH_2Cl_2 was purchased from Kanto as anhydrous solvent and was stored in the presence of 4A molecular sieves. To remove a trace of HCl, CH_2Cl_2 was passed through activated alumina under an Ar atmosphere just before use. Tetrabutylammonium perchlorate was purchased from Kanto and was dried over P_2O_5 in vacuo. CD_3OD was purchased from ACROS and was dried over 3A molecular sieves. CD_2Cl_2 was purchased from ACROS and was stored in the presence of 4A molecular sieves. CD_2Cl_2 was also passed through activated alumina under an Ar atmosphere just before use. ^{57}Fe metal (95.40%) was purchased from ISOFLEX. The oxidant **5** was prepared according to the reported method[34] and was assayed with titration by ferrocene. *m*CPBA was purchased from Nacalai and was purified by washing with a phosphate buffer.[35] ^{18}O-labeled *m*CPBA was prepared according to the reported method.[36] Purity of *m*CPBA was checked with iodometry. Other reagents were purchased from Kanto or Aldrich and were used as received.

Synthesis. Preparations of **1** and **2** have been already reported.[18]

3. To the complex **1** (50 mg, 45 μmol) in anhydrous THF (0.5 mL) was added NaOEt (3.1 mg, 45 μmol) in anhydrous EtOH (5 mL). The solution was stirred at room temperature for 10 min, yielding a reddish precipitate. The resulting precipitate was filtered out and washed with a small amount of EtOH. The precipitate was dissolved in hexane and was passed through a membrane filter (pore size 0.5 μm) to remove a trace of NaCl. Recrystalization from hot EtOH gave a red crystalline product of **3** (35.7 mg, 33 μmol). Anal. Calcd for $[C_{72}H_{79}FeN_2O_3](H_2O)$: C, 79.03; H, 7.46; N, 2.56. Found: C, 78.68; H, 7.31; N, 2.59.

4. The solution of **4** was prepared by dissolving **2** (4.37 mg, 3.69 μmol) in 0.1 M tetrabutylammonium perchlorate/CH_2Cl_2 (3.7 mL) containing 2.5 equiv of tetrabutylammonium hydroxide (7.38 mg, 9.23 μmol) and utilized without purification.

The iron salen complex bearing the CD_3O group was prepared in exactly the same manner using $NaOCD_3/CD_3OD$ instead of NaOEt/EtOH. Anal. Calcd for $[C_{71}H_{74}D_3FeN_2O_3](H_2O)_2$: C, 77.43; H, 7.69; N, 2.54. Found: C, 77.71; H, 7.33; N, 2.64.

^{57}Fe-enriched **1** was synthesized from $^{57}Fe(OAc)_2$, which was prepared from ^{57}Fe metal (95.40%) and acetic acid. ^{57}Fe-enriched **2** was prepared from ^{57}Fe-enriched **1** according to the preparation of **2**.[18]

UV−Vis Measurements upon Controlled-Potential Electrochemical Oxidation. Controlled-potential electrochemical oxidation was conducted in a thin-layer quartz cell (0.05 cm) using a gold-mesh working electrode, a platinum-wire counter electrode, and an Ag/AgCl reference electrode, which are connected to a HA-151 potentiostat-galvanostat (Hokuto Denko). The quartz cell was cooled at 203 K, and then the constant potential was applied at the voltage which was higher by 150 mV than the first oxidation potential. UV−vis spectral changes were monitored during electrochemical oxidation to confirm generation of $[\mathbf{1}]^+$ and $[\mathbf{2}]^+$ after 2 h. Then, $[\mathbf{1}]^{2+}$ and $[\mathbf{2}]^{2+}$ were generated after an additional 2 h by controlled potential oxidation at the voltage that was higher by 300 mV than the second oxidation potential.

Preparative Electrochemical Oxidation. Exactly the same method described above was employed except for utilization of a 0.1 cm thin-layer quartz cell. After formation of one- and two-electron-oxidized intermediates was confirmed with UV−vis spectroscopy, the electrodes were removed from the quartz cell. The intermediate solution was carefully transferred via a cooled gastight syringe to an EPR sample tube or a reaction tube to measure EPR or investigate reactivity.

Mössbauer Measurements. Mössbauer spectra were measured with a conventional spectrometer in the constant-acceleration mode. Isomer shifts were reported relative to metallic iron (α-Fe) at room temperature. Mössbauer spctra were measured for ^{57}Fe-enriched complexes. The sample solution was prepared at 203 K in a test tube and then transferred via a precooled gastight syringe to a Teflon Mössbauer cell. Immediately, a Mössbauer cell was immersed in a liquid-nitrogen bath and then attached to the sample holder. To obtain clear spectra for samples in CH_2Cl_2, data were accumulated for 3−7 days. Simulation was conducted without any restriction.

Low-Temperature ESIMS. To obtain mass spectra of transient species, both desolvation and nebulizer gas were cooled with liquid nitrogen. The sample solution was prepared in a test tube at 203 K, and a portion of the solution was diluted with CH_2Cl_2 in a gastight syringe cooled with dry ice. The sample solution was then transferred to the inlet of the mass spectrometer through precooled capillary tubing.

Chemical Oxidation of 1 by 5. For Mössbauer, resonance Raman, and ESIMS measurements of $[\mathbf{1}]^+$ and $[\mathbf{1}]^{2+}$, chemical oxidation by **5** was employed. Preparation of the resonance Raman sample is described as a representative procedure: To the solution of **1** (1.92 mg, 1.80 μmol) in CH_2Cl_2 (0.6 mL) in an acetone−CO_2 bath was added 1.0 or 2.0 equiv of **5** (2.11 mg, 1.80 μmol, or 4.21 mg, 3.60 μmol) in CH_2Cl_2 (0.4 mL). $[\mathbf{1}]^+$ and $[\mathbf{1}]^{2+}$ were generated immediately

***m*CPBA Oxidation of 2.** Preparation of the UV−vis sample is described as a representative procedure: To the CH_2Cl_2 solution of **2** (1.67×10^{-4} M, 1.8 mL) in a UV−vis cell at 193 K was added a CH_2Cl_2 solution of *m*CPBA (1.5×10^{-3} M, 0.2 mL). The mixture was stirred at 193 K for 5 min, and then a UV−vis spectrum was measured.

Quantitative Analysis. The yield of bezaldehyde was determined with a QP5000 GC-MS (Shimadzu), using benzophenone as an internal standard. Quantitative analysis of acetaldehyde was carried out by the reported method.[37] The net yield of acetaldehyde was calculated, considering the blank test under exactly the same conditions. Each quantitative analysis was repeated three times, and the average values were reported.

Acknowledgment. We thank Mr. S. Makita in our Institute for elemental analyses. We also thank Equipment Development in our Institute for preparation of the Mössbauer cell. This work was supported by a Grant-in Aid for Scientific Research from the Ministry of Education, Culture, Sports, Science, and Technology of Japan.

IC051377E

(34) Schmidt, W.; Steckhan, E. *Chem. Ber.* **1980**, *113*, 577−585.
(35) Schwartz, N. N.; Blumbergs, J. H. *J. Org. Chem.* **1964**, *29*, 1976−1979.
(36) Wagner, W. R.; Rastetter, W. H. *J. Org. Chem.* **1983**, *48*, 402−404.
(37) Miyake, T.; Shibamoto, T. *J. Agric. Food Chem.* **1993**, *41*, 1968−1970.